# COMPUTATIONAL FLUID DYNAMIC ANALYSIS ON SOLAR WATER HEATER
## Role of Thermal Stratification and Mixing on Dynamic Mode of Operation

by

***Karuthedath DILEEP[a*], Arun RAJ[b], Divakaran DISHNU[b], Ahamed SALEEL[c], Mokkala SRINIVAS[b], and Simon JAYARAJ[b*]***

[a] Department of Production Engineering, VAST, Thrissur, Kerala, India
[b] Solar Energy Center, Department of Mechanical Engineering, NITC, Kerala, India
[c] Mechanical Engineering Department, College of Engineering, King Khalid University, Abha, KSA

Original scientific paper
https://doi.org/10.2298/TSCI190601419D

*The present work attempts to demonstrate the competence and reliability of the proposed computational solver for real-scale modelling and analysis of a commercially available evacuated tube collector type solar water heater. A 3-D, transient numerical solver with user-defined functions is modelled using CFD program ANSYS-Fluent 15.0®. The objective is to analyse the evacuated tube collector type solar water heater in two states of operation, namely, static (stagnant charging) and dynamic (retrieval) modes. This work emphasizes the determination of the impact of thermal stratification, and fluid mixing in the storage tank on the outlet temperature profile during discharging. Volume flow rates vary from 3-15 Lpm. The reported findings suggest that with an increase of fluid-flow during discharge, the stratified layers disorient and lead to rapid mixing, which eventually results in an earlier drop in the outlet water temperature. Furthermore, at low fluid-flow rates, the stratified layers remain intact with only a gradual decay in the outlet temperature profile. The analysis reveals that based on the user's choice, it is possible to vary discharge flow rate until 7 Lpm without a significant drop in the outlet water temperature. Furthermore, computational results have been successfully validated with experimental findings.*

Key words: *CFD, finite volume method, stratification, solar water heater, evacuated tube collector*

## Introduction

Effective solar energy utilization is the focal point of rigorous research, which aims to bring out competent and reliable technological advancements with an emphasis on safeguarding the natural resources and for counteracting carbon-emissions [1]. Accessible, ubiquitous, economical, and pollutant-free attributes of solar energy favour its widespread use. These traits have led to the vast popularity of solar thermal applications, in spite of the intermittency and low energy density of solar radiation on the earth surface [2]. Air and water heating, space heating, desalination, humidification-dehumidification, drying, seasoning of timber, and processes heating are among the top listed solar thermal applications [3]. In the present global market, the solar water heater (SWH) is a booming appliance with rapid commercialization. Pressurized

* Corresponding authors, e-mail: sjayaraj@nitc.ac.in

and non-pressurized SWH variants [4] are of user's choice and depend on the meteorological conditions. Non-pressurized SWH comprises of flat plate collectors (FPC) and evacuated tube collectors (ETC). Evacuated tube collector type solar water heater (ETCSWH) is a common choice of non-pressurized SWH for domestic and small-scale sectors with hot water requirement [5]. An ETCSWH encompasses set of ETC tubes, a storage tank, and insulation. The ETCSWH has inherent advantages of zero conductive or convective losses and better performance even at low solar intensities. In principle, the SWH absorbs the incident solar radiation, and stores it as sensible heat. However, there exists a perception among the people that, the SWH system is economically non-profitable. Eventhough it runs on near-zero operational cost, higher initial cost and installation difficulties have led to this perception.

Rout *et al*. [6] performed a detailed economic analysis using Monte Carlo simulation and net present value (NPV) tool. The NPV based on eight dynamic variables assures the competence of domestic SWH as a viable option irrespective of its high initial investment cost. Peres [7] experimentally investigated the long-term performance of an FPC and an ETC based SWH system under the meteorological conditions of Sweden. The reported findings suggest that the ETC had better performance in comparison with that of the FPC based SWH system. Zambolin and Col [8] presented a theoretical and experimental analysis to determine the daily efficiency of a flat-plate and an ETC based SWH. The observed findings suggest that ETC based SWH has higher efficiency over wide operating conditions with limited heat losses. Sokhansefata *et al*. [9] reported a thermo-economic analysis performed on a flat-plate and an ETC based SWH system. The TRNSYS-16 software predicted the annual collector energy output and the outlet temperature. The ETC based SWH system was economical and outperformed the FPC system by 41%. Budihardjo and Morrison [10] presented an experimental and numerical analysis to determine the optical and heat loss characteristics of evacuated tube SWH. The results suggest that the tank size was less significant for evacuated collectors in comparison with FPC. Morrison *et al*. [11] performed numerical simulations on a long single-ended thermosyphon tube. The obtained results reported the presence of an inactive region closer to the sealed end of the tube, which possibly affects the performance of ETCSWH. Yildizhan and Sivrioglu [12] made an energy and exegy analysis on a vacuum tube solar collector and concluded that the efficiencies primarily depended up on the solar irradiance and ambient temperature has greater influence on the the exergy efficiency. Thermal stratification in a thermosiphon SWH was investigated experimentally by Riahi and Taherian [13] Satisfactory state of thermally stratified layers was observed with a maximum temperature of 68 °C in the topmost stratified layer in the experiment.

Zeghib and Chaker [14] developed a numerical model of a domestic solar water heating system. Their results indicate the influence of thermosyphon effect and the degree of stratification inside the storage tank. Nitsas and Koronaki [15] performed experimental and theoretical analysis to investigate the charging characteristic of an ETC based SWH system. The analysis emphasized to evaluate the collector performance using First and Second law efficiencies. The results convey that the inlet water temperature significantly influences the thermal and exergy efficiency of the system. The analysis did not account for the discharging characteristics of the system. Abdelhak *et al.* [16] presented a computational analysis using FLUENT v6.3® software. The study aimed to determine the dynamic thermal response of a domestic hot water storage tank. The results suggest that the tank orientation (horizontal/vertical) significantly affects the evolution of the stratified layers within the tank. Furthermore, vertical orientation proved to be advantageous than the horizontal tank configuration. Levers and Lin [17] numerically analyzed the influence of tank geometry (varying height and aspect ratio) and the operating conditions

on the thermal stratification within a storage tank using FLUENT® software. The result conveyed that the tank with the highest aspect ratio performed the best. However, the performance improvement recorded was marginal beyond an aspect ratio of 3.5. The effect of changing the position of inlet/outlet along with mass-flow rate revealed that a higher mass-flow rate often paved the way to destroy the thermally stratified layers. Lavan and Thompson [18] experimented on a cylindrical hot water tank positioned vertically to study the effects of stratification. The experiments conducted at different flow rate revealed that stratification occurs even at a higher flow rate. The flow when directed towards the wall resulted in better performance. Assari *et al*. [19] performed numerical and experimental studies to determine the effect of inlet position on the storage tank of the collector. The obtained results confirmed that the provision of the water inlet to the top of the storage tank resulted in maximum stratification. In particular, with the thermosyphon systems, provision of the water inlet at the top and exit at the bottom proves to be beneficial. Fernandez-Seara *et al.* [20] conducted an experimental investigation on a domestic electrical water heater on two modes of operation, namely, static and dynamic mode. Based on six possible inlet-outlet port positions on the storage tank and at flow rates of 5 Lpm, 10 Lpm, and 15 Lpm, the conducted experiments identified the optimum configuration that yielded better performance. Shah and Furbo [21] presented a theoretical and experimental analysis to study the thermal behaviour of water jets entering a solar store. Furthermore, a numerical analysis conducted based on three inlet designs and with different inlet flow rates aided to determine the thermal performance.

In general the stated literature, experimental, theoretical, and numerical studies on SWH discussed the influence of storage tank orientation (horizontal/vertical), the effect of mixing, the impact of inlet-outlet ports provided on the storage tank, and mass-flow rate on the thermal stratification. Furthermore, the literature survey presented here discussed the advantages of ETCSWH systems over FPC systems. In the present work, the authors put forth a computational solver with capabilities for real-scale modelling and analysis of a commercially available ETCSWH. This work aims to visualize the thermal gradient developed within the storage tank during the charging mode as well as to determine the role of thermal stratification during the discharging mode of operation of the ETCSWH. Based on our knowledge and available literature survey, there is an inadequacy of computational studies that take into account of the entire ETCSWH for real-scale modelling and transient analysis to determine the influence of thermal stratification on the overall performance of the collector.

## Description of experiment

A commercially available ETCSWH system manufactured by M/s. Orb Energy, Bangalore installed in the Solar Energy Center (SEC) of National Institute of Technology Calicut (11° 32′ N, 75° 93′ E), India facilitates to perform the experimental investigation. The entire experimental work comprises of two major segments, namely, the charging and the discharging modes of operation. The present analysis made use of the experiments performed under clear sky conditions for comparison.

### *Lay-out of experimental set-up and measurements*

The ETCSWH comprises a horizontal storage tank (100 liters volume), evacuated tubes, and thermal insulation. An overhead tank supplies water to the ETCSWH. Figure 1 shows the experimental set-up used for the present analysis. The storage tank is made of mild steel. Twelve evacuated tubes connected to the storage tank with a 30° inclination with the horizontal receive the incident solar radiation. Evacuated tubes made using borosilicate glass enable the

collector to withstand high temperatures. Rubber pads support the bottom ends of the evacuated tubes. An inlet port positioned at bottom end on one side of the storage tank supplies water to the ETCSWH. Similarly, an outlet port situated at the top end on the opposite side of the tank facilitates water discharge. Commercially available SWH systems adopted such inlet-outlet port positioning to favor the thermal stratification phenomenon. Polyurethane foam insulation (0.05 m thick) provided throughout the circumference of the tank, which helps to minimize the heat leakage. Table 1 describes the geometrical details of the experimental set-up. Davis-Vantage Pro2 weather station installed at the SEC records the meteorological data continuously at regular intervals (every 60 seconds) using a Weather-Link program monitored by a PC-based system. The ambient temperature recorded by the weather station has an accuracy of 0.5 °C. An industrial standard pyranometer measures the incident solar radiation with a nominal accuracy of 5 W/m$^2$. Five K-type thermocouples connected to an Agilent data monitoring system measures temperature at various locations within the ETCSWH. Figure 2 shows the arrangement of thermocouple positioned diametrically within the storage tank to determine the temperature distribution during the experimentation. The nominal accuracy of temperature measurement is 0.5 °C. A conventional measuring beaker and stopwatch are used to estimate the water discharge through the outlet port.

**Figure 1. Photograph of the ETCSWH**

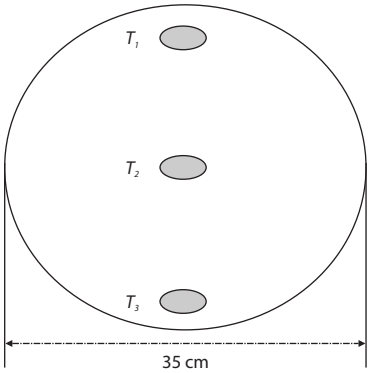


**Figure 2. Thermocouple positions**

**Table 1. Details of experimental set-up**

| Parameter | Dimensions |
|---|---|
| Tank diameter | 35 cm |
| Tank length | 100 cm |
| ETC tube diameter | 4.2 cm` |
| ETC tube length | 160 cm |
| Tank volume | 100 l |
| Inlet/outlet port diameter | 2.54 cm |
| Angle of inclination | 30° |

### *Experimental procedure*

In principle, the incident solar radiation on the evacuated tubes of the collector is absorbed and transferred the energy to the working fluid (water) by conduction and convection. As the ETCSWH is a non-pressurized system, temperature gradient aided natural-convection facilitates re-circulation within the tubes. It results in the accumulation of hot water at the top portion of the storage tank. As time progresses, the water within the storage tank gets heated up, and its rate of utilization is user dependent. In general, an experiment on ETCSWH comprises the charging and the discharging modes of operation. During the charging mode, the ETCSWH absorbs the incident solar radiation without any interruption from 7:00 a. m. to 6:30 p. m. under the static mode (no inflow and outflow from the tank). During the discharging

mode (or the dynamic mode), which occurs beyond 6:30 p. m., the water discharges through the outlet port at a constant flow rate. The proposed period for charging and discharging resembles a domestic household scenario where (in general) there is no hot water consumption requirement during the daytime. During every 15 minutes, the data acquisition system records the temperature distribution in the charging mode, and at every 15 seconds in the discharging mode of operation. In the dynamic mode (discharging), the cold water (ambient) from the overhead tank enters the ETCSWH. A proportionate amount of hot water collected at the outlet serves the domestic requirements. The discharging mode continues until the temperature of hot water drops to 35 °C. For the sake of simplicity, a temperature of 35 °C, which is close to the peak ambient temperature at the current location during charging, is set as the datum. For numerical validation purpose, the temperature history during the charging and discharging modes of operation is of interest. The discussed experimental findings correspond to water run off (during discharging mode) at a constant volume flow rate of 3 Lpm. Hence, in the present work, the experimentation work limits itself and does not perform the overall thermal performance calculation of the ETCSWH.

## Description of numerical work

### *Geometry and mesh*

The Design modeler package in ANSYS® facilitates to model a real-scale 3-D model of a standard ETCSWH system. The computational model is analogous to the description of ETCSWH done in *Layout of experimental set-up and measurements* and the details provided in tab. 1. Figure 3 shows the computational domain used for the present work. The ICEM-CFD package in ANSYS® aids for the discretization of the computational domain. The surface mesh generated initially act as the datum for volume meshing under the Delaunay scheme. The inlet-outlet ports and the evacuated tubes contain finer mesh elements. Figure 4 depicts the meshed geometry of the computational domain used in this analysis. However, a grid independence test conducted ensured the accuracy of the results obtained from the

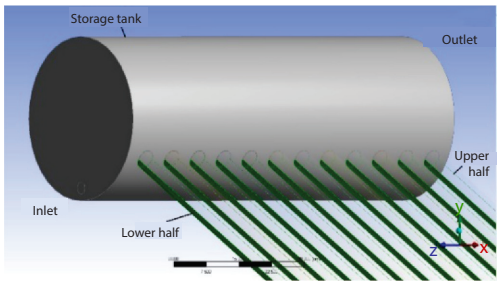


**Figure 3. Computational domain**

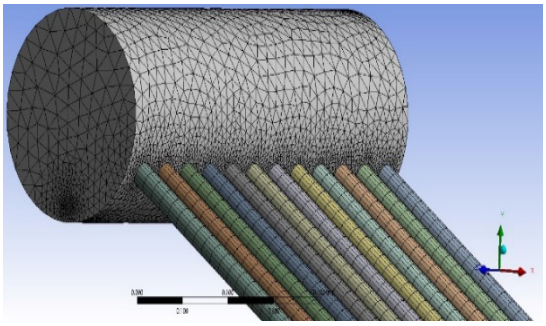

**Figure 4. Mesh used for the present work**

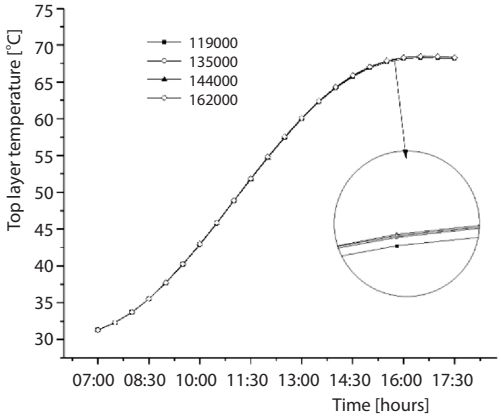


**Figure 5. Results of the grid independence test**

present analysis. Figure 5 describes the details of the different mesh elements chosen for the analysis. The results suggested that a total of 147588 elements is the optimum mesh for the present work. Furthermore, the orthogonal quality and mesh skewness of the selected mesh were under the prescribed limits.

### *Governing equations*

Most of the complex fluid-flow and heat transfer problems consist of coupled non-linear PDE that are tedious and cumbersome mathematically. They require rigorous mathematical procedures to obtain the correct solution [22]. In this study, a transient, 3-D, incompressible, Newtonian, laminar numerical solver with body force term and user-defined function (UDF) facilitating the numerical computation. Equations (1)-(4) describe the conservation equations and correlations used in the present calculation. The Fluent package in ANSYS® based on the finite volume method discretizes the governing equation. In the current analysis, the major assumptions involved are:

– Thermophysical properties of the fluid are constant except for density.
– Boussinesq approximation accounts for the natural-convection inside the evacuated tubes.
– Viscous dissipation is negligible.
– No heat losses occur through the bottom ends of evacuated tubes.

Using these assumptions the governing equations, that are, continuity, momentum and energy equations are written:

$$\frac{\partial \rho}{\partial t} + \nabla(\rho \vec{\mathrm{V}}\vec{\mathrm{V}}) = 0 \tag{1}$$

$$\frac{\partial(\rho \vec{\mathrm{V}})}{\partial t} + \nabla(\rho \vec{\mathrm{V}}\vec{\mathrm{V}}) = -\nabla p + \mu(\nabla^2 \vec{\mathrm{V}}) - \mathrm{g}\beta(T_\mathrm{s} - T_\mathrm{ref}) \tag{2}$$

$$\frac{\partial(\rho H)}{\partial t} + \nabla\left(\rho \vec{\mathrm{V}} H\right) = \nabla(k \nabla T) + S_h \tag{3}$$

where $\beta$ refers to the coefficient of thermal expansion and $S_h$ stands for the energy source term. Equation (4) accounts for the heat loss through the insulation from the storage tank walls and has a following form.:

$$\frac{2\pi k L \Delta T}{\ln \dfrac{r_2}{r_1}} + \frac{2k A_\mathrm{c} \Delta T}{\Delta x} = UA\Delta T \tag{4}$$

where $k$ [Wm$^{-1}$K$^{-1}$] is the thermal conductivity, $\Delta T$ [Wm$^{-2}$K$^{-1}$] – the temperature difference between the water inside the storage tank and the ambient, and refers to the overall heat transfer coefficient.

### *Boundary conditions and numerical schemes*

In this work, the numerical computation is in line with the experimental studies performed. The present computation consists of two modes of operation, namely, the stagnant mode (charging) and the dynamic mode (discharging) of operation. In the stagnant mode, there is no inflow or outflow from the ETCSWH. However, in the dynamic mode, the water drains through the outlet port as fresh water from the overhead tank enters at a constant flow rate through the inlet port of the ETCSWH. Hence, in the charging mode, the inlet and outlet port velocity is zero, and the solar radiation falls on the collector tubes. During the discharging

mode, the inlet port has a fixed mass-flow inlet condition with the inlet temperature fixed as 30 °C. During this mode of operation (*i. e.*, beyond 6:30 p. m.), the incident solar radiation intensity on the collector tubes is zero. During the charging mode, in order to mimic the real-scale scenario, the numerical analysis utilizes the recorded incident solar radiation data over the collector during experimentation. The curve-fitting tool in MATLAB® converts the incident solar radiation based on the experimental observations and applies it as a UDF (fourth order polynomial) to the evacuated tube walls. It has to be noted that the evacuated tube surface is split in two parts, namely, the upper half and the lower half, respectively. The upper half of the evacuated tubes absorbs the direct and diffuse solar radiation whereas the lower half absorbs the reflected radiation from the concrete floor (floor space of installation). Demain *et al.* [23] evaluated different models to estimate the radiation components on an inclined surface under varying sky conditions. The ratio of contributions of direct component of irradiance on an inclined surface with the global radiation ranged from 28-61% and that of reflected varied from 14-16% under different sky conditions.

In this work, the pressure implicit with splitting of operator (PISO) algorithm facilitates to solve the pressure-velocity coupling in the N-S equation. The pressure, time derivative terms, momentum, and energy utilize the PRESTO algorithm, first-order temporal schemes, and the second-order upwind schemes for the numerical discretization. Default values of under-relaxation factors help the numerical solver to obtain iterative convergence. The scaled-residuals set for all conservation equations were $10^{-3}$ except for the energy equation, which was $10^{-6}$. Furthermore, the reported resulting imbalances during post-processing were less than 1%. Monitors provided at different locations in the ETCSWH during the numerical computation continuously tracked and recorded the temperature distribution of the storage tank and the outlet temperature.

### *Validation of the numerical solver*

For the numerical validation, the experimental work conducted on the ETCSWH at SEC on the clear day of November 21, 2018 act as the datum. The primary factor influencing the temperature distribution within the ETCSWH is the incident solar radiation. Hence, to mimic the variation in solar radiation intensity, a variable heat flux condition is applied on the evacuated tube walls identical to the recorded solar radiaton intensity (November 21, 2018) from the weather station with the help of a UDF. During the discharging mode of operation, the selected value of constant volume flow rate was 3 Lpm. The remaining boundary conditions applied to the computational domain are as mentioned in *Boundary conditions and numerical schemes*. Figure 6 shows the comparison of temperature variation on the top, center, and the bottom portion of the ETCSWH during the charging mode of operation. The observations conveyed

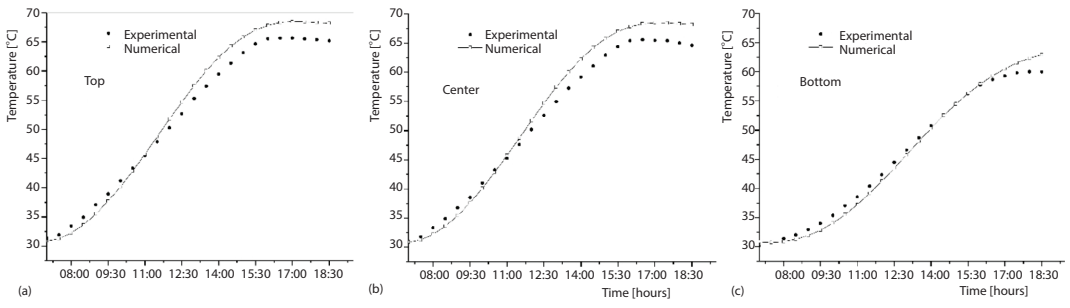


**Figure 6. Comparison of temperature at different locations within the tank during charging**

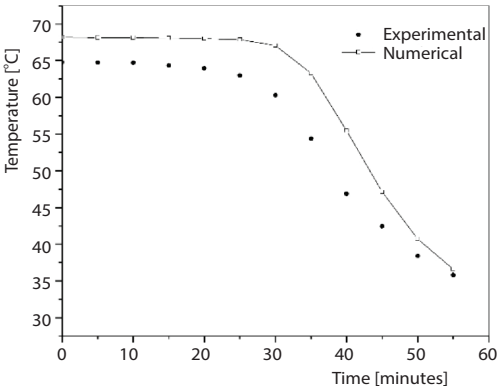


**Figure 7. Comparison of outlet temperature profile during discharging**

that the obtained trend of the numerical results match with that of the experimental findings.

Figure 7 shows the comparison of the outlet temperature variation of the ETCSWH during the discharging mode of operation. The difference in the slope observed between the curves conforms to the lower mixing in the storage tank during the numerical analysis. The results indicate that there is a close agreement between the numerical and experimental findings as observed in the charging mode of operation. This is similar in lines with Zelzouli *et al.* [24] who validated their numerical model with the experimental findings and obtained a matching trend during the discharging mode of operation.

## Results and discussion

### *Experimentation on ETCSWH*

As mentioned in *Validation of the numerical solver*, the discussed experimental observations correspond to the clear day on November 21, 2018. Figures 8 and 9 describes the temperature distribution at different locations within the storage tank during charging and discharging modes of operation. In the charging mode, as the solar radiation falls over the collector tubes, the water absorbs the heat, recirculates through the upper half of the tubes, and accumulates at the top portion of the storage tank. The sole reason attributes to the density difference between the hot and cold water within the storage tank of the ETCSWH. Figure 8 revealed that the temperature at the center and the top remains almost the same during the charging process. It is due to the continuous re-circulation occurring within the storage tank. However, the temperature at the bottom portion of the tank is lower than that of the middle and the top portion. The observed behavior accounts possibly due to the stagnant water present at the bottom portion of the storage tank of the ETCSWH attributed to the inclination provided for maximum solar absorption. Furthermore, as observed, the temperature increases proportionally to the inci-

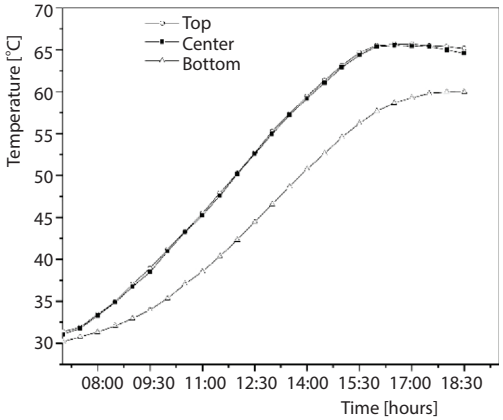


**Figure 8. Temperature profiles within tank during discharging (Experimental)**

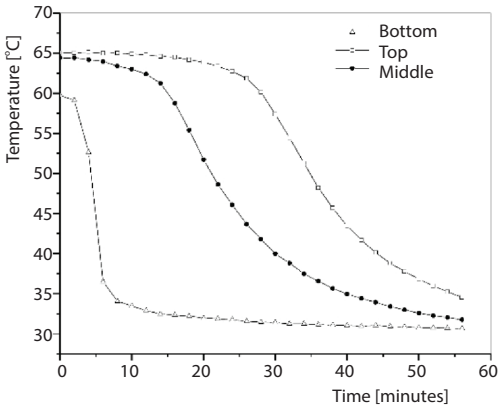


**Figure 9. Temperature profiles within the the tank during charging (Experimental)**

dent solar radiation over the collector. However, beyond 4:00 p. m., the observed gradual dip in the temperature rise is due to the sudden drop in solar intensity. Figure 9 shows the temperature profile at different locations during the discharging mode of operation. As expected, the temperature at the bottom portion of the tank drops immediately with the inflow of the cold water from the overhead tank. However, the temperature at the center and top portion decreased gradually due to the presence of thermally stratified layers created during the charging mode. The maximum outlet temperature recorded was 65 °C. At a constant flow rate of 3 Lpm, the outlet temperature of hot water obtained was consistent for almost 30 minutes. The inlet-outlet port positions thus favor the hot water extraction without further mixing due to the inflow during the discharging mode.

## Numerical results of ETCSWH

During the charging mode, the temperature profile obtained at different locations within the tank was similar to the results obtained from the experimental findings. Figures 10 and 11 show the temperature contours and velocity vector plots, respectively, during the charging mode. The contours indicate the temperature profiles created within the storage tank as stated in *Experimentation on ETCSWHS*. As mentioned, the numerical results match with the experimental observations, which claim that the lower temperature at the bottom portion is due to the presence of a stagnant region at the lowermost part of the tank. Moreover, the vector plots help to visualize the natural-convection effects/re-circulation occurring within the evacuated tubes. However, the main purpose of this study is to determine the effect of discharge rate on the outlet temperature profile. Hence, the numerical work discusses the detailed analysis performed on the dynamic mode of operation. The analysis makes use of five different flow rates (*i. e.*, 3, 5, 7, 10, and 15 Lpm) for the comparative study. However, a dimensionless time, $t^* = t/t_{35}$, has been introduced to simplify the comparative study. Here $t$ is the actual time and $t_{35}$ corresponds to the time for which the outlet temperature attains 35 °C. Figure 12 shows the outlet temperature history corresponding to dimensionless time, $t^*$, at different flow rates. Initially at the start, for all cases, the outlet temperature remains constant. However, as time progress the outlet temperature drops due to mixing occurring due to the inflow of cold water. The observed temperature drop is immediate for 15 Lpm in comparison with 3 Lpm. The abrupt deviations noticeable corresponding to 15 Lpm may be possibly due to the sudden mixing occurring within the tank, which breaks the thermally stratified layers. For 10 Lpm, the outlet temperature showed a similar trend. Furthermore, for the intermediate cases such as 5 and 7 Lpm, the observed outlet temperature history is similar to 3 Lpm itself. This suggests that it is favor-

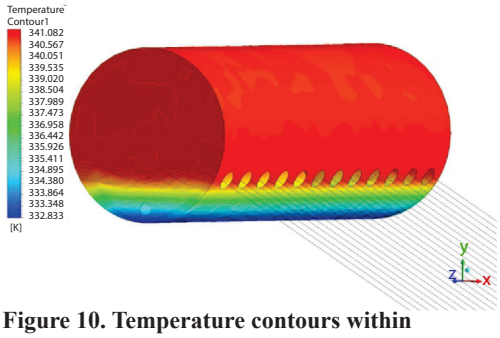


**Figure 10. Temperature contours within the storage tank during charging** (*for color image see journal web site*)

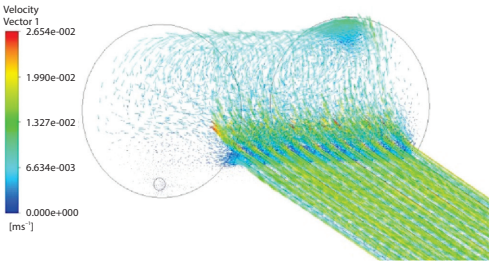


**Figure 11. Velocity vector plots within the ETCSWH** (*for color image see journal web site*)

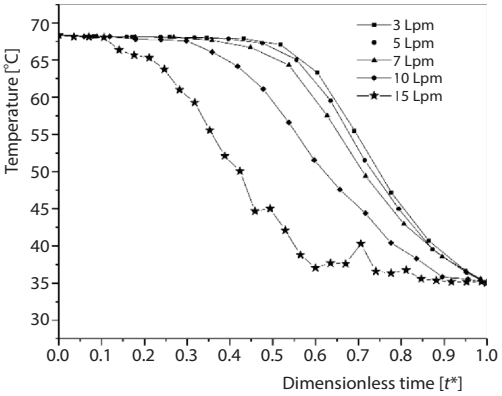


**Figure 12. Outlet temperature profile corresponding to the dimensionless time**

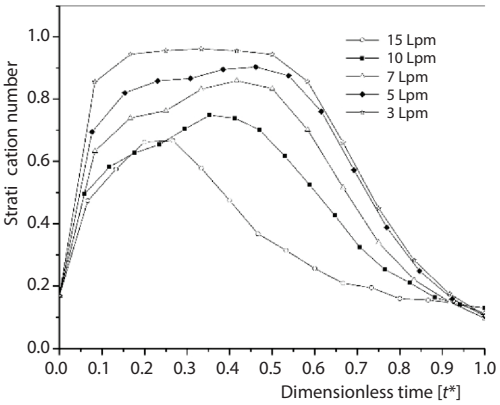


**Figure 13. Comparison of stratification number corresponding to different flow rates**

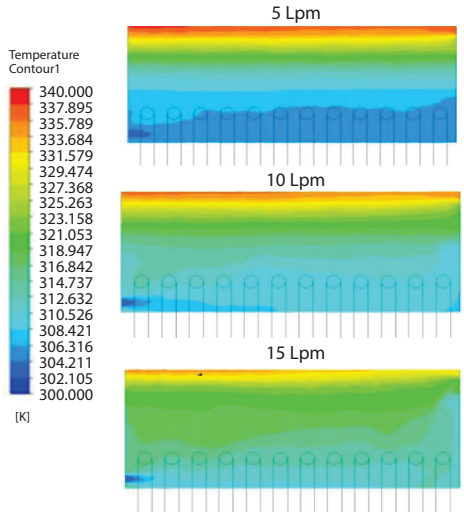


**Figure 14. Temperature contours along an axial plane cut through the ETCSWH** (*for color image see journal web site*)

able to increase the flow rate from 3 to 7 Lpm without sacrificing the outlet temperature. Fernandez-Seara *et al.* [20] introduced the stratification number (*Str*, non-dimensional) which represents the strength of thermally stratified layers. In general, a high value corresponds to greater magnitude of stratification and zero value corresponds to a uniform temperature distribution within the tank. Equations (5) and (6) define the stratification number, *Str*, as:

$$Str = \left(\overline{\partial T / \partial Z_t}\right) / \left(\overline{\partial T / \partial Z_0}\right) \tag{5}$$

$$\overline{\partial T / \partial Z} = \frac{1}{J-1}\left[\sum_{J=1}^{J-1}\left(\frac{T_{J+1} - T_J}{\Delta z}\right)\right] \tag{6}$$

Figure 13 shows the stratification number corresponding to different discharge flow rates. The trend observed revealed that 3 Lpm was able to sustain the value closer to one for a longer duration, when compared to the other flow rates. As the flow rate increases, maximum attainable value decreases for all flow rates. Fernandez-Seara *et al.* [20] discussed similar variation in the stratification number during the dynamic mode of operation conducted at variable flow rates of 5 Lpm, 10 Lpm, and 15 Lpm. Abdelhak *et al.* [16] also studied the effect of thermal stratification using the stratification number, *Str*.

Figure 14 shows the contours of temperature distribution across an axial plane cut through the ECTSWH. The contours correspond to the stage when 90 liters of water discharged from the tank.

## Conclusion

This work addresses the lack of computational studies performed on a full-scale model of an ETCSWH during the discharging mode of operation. The work discusses the experimental and numerical studies conducted on ETCSWH available in the market. The primary objective is to develop a computational solver with capability for real-scale modelling and analysis of ETCSWH. Additionally, the study seeks to determine the role of discharge rate on

the outlet temperature variation under the influence of fluid mixing and thermal stratification. In general, the whole analysis comprises of two modes of operation, namely, the charging (static) and the discharging (dynamic) mode. A transient, 3-D, pressure based, Newtonian, laminar solver with UDF facilitates the numerical computation. The experimental findings act as the datum to validate the proposed numerical solver. The numerical results were in close agreement with that of the experimental findings. The numerical work took into consideration five different discharge flow rates (*i. e.*, 3, 5, 7, 10, and 15 Lpm ) to determine the effect on outlet temperature profile during the dynamic mode of operation. The results conveyed that up to a limiting value of 7 Lpm, the outlet temperature profile did not decay abruptly as that of 10 Lpm and 15 Lpm. Similarly, the value of stratification number, *Str*, indicated that as the flow rate increases, the maximum attainable value decreases. Hence, during the discharging mode, based on the user requirement, the flow rate can vary from 3-7 Lpm without sacrificing the outlet temperature. Furthermore, the authors were successful in visualizing the flow behavior as well as in demonstrating the thermally stratified layers evolved within the storage tank in the present work.

## Nomenclature

$A$ – area, [m$^2$]
$C_p$ – specific heat capacity at constant pressure, [Jkg$^{-1}$K$^{-1}$]
g – acceleration due to gravity, [ms$^{-2}$]
$H$ – enthalpy, [Jkg$^{-1}$]
$J$ – number of water layers
$k$ – thermal conductivity, [Wm$^{-1}$K$^{-1}$]
$L$ – length, [m]
$p$ – pressure, [Pa]
$r$ – radius, [m]
*Str* – stratification number
$T$ – temperature, [°C]
$U$ – overall heat loss coefficient, [Wm$^{-2}$K$^{-1}$]
$\vec{V}$ – velocity vector, [ms$^{-1}$]
$\Delta x$ – hickness of insulation, [m]
$z$ – heigh, [m]
$\Delta z$ – distance between two nodal points, [m]

*Greek symbols*

$\beta$ – coefficient of thermal expansion, [K$^{-1}$]
$\rho$ – density, [kgm$^{-3}$]
$\mu$ – dynamic viscosity, [Pa·s]

*Acronyms*

ETCSWH – evacuated tube collector based solar water heater
FPC – flat-plate collector
PRESTO – pressure staggering options

*Subscripts*

c – cross-section
j – nodal points
s – surface
ref – reference

## Acknowledgment

The authors also gratefully acknowledge the funding provided by the Deanship of Scientific Research at King Khalid University, Kingdom of Saudi Arabia for funding this work through research groups program under the grant number (R. G. P. 1/87/40) in connection with the present work.

## References

[1] Tian, Y., Zhao, C. Y., A Review of Solar Collectors and Thermal Energy Storage in Solar Thermal Applications, *Applied Energy*, *104* (2013), Apr., pp. 538-553
[2] Raj, A. K., *et al*., A Cost-Effective Method to Improve the Performance of Solar Air Heaters Using Discrete Macro-Encapsulated PCM Capsules for Drying Applications, *Applied Thermal Engineering, 146* (2019), Jan., pp. 910-920
[3] Zalba, B., *et al*., Review on Thermal Energy Storage with Phase Change: Materials, Heat Transfer Analysis and Applications, *Applied Thermal Engineering*, *23* (2003), 3, pp. 251-283
[4] Islam, M. R., *et al*., Solar Water Heating Systems and Their Market Trends, *Renewable and Sustainable Energy Reviews*, *17* (2013), Jan., pp. 1-25

[5] Sabiha, M. A., *et al*., Progress and Latest Developments of Evacuated Tube Solar Collectors, *Renewable and Sustainable Energy Reviews*, *51* (2015), Nov., pp. 1038-1054
[6] Rout, A., *et al*., Risk Modelling of Domestic Solar Water Heater Using Monte Carlo Simulation for East-Coastal Region of India, *Energy*, *145* (2018), Feb., pp. 548-556
[7] Perers, B., Comparison of Thermal Performance for Flat Plate and Evacuated Tubular Collectors, *Advances In Solar Energy Technology*, (1988), Sept., pp. 615-619
[8] Zambolin, E., Del Col, D., Experimental Analysis of Thermal Performance of Flat Plate and Evacuated Tube Solar Collectors in Stationary Standard and Daily Conditions, *Solar Energy*, *84* (2010), 8, pp. 1382-1396
[9] Sokhansefat, T., *et al*., Thermoeconomic and Environmental Analysis of Solar Flat Plate and Evacuated Tube Collectors in Cold Climatic Conditions, *Renewable Energy*, *115* (2018), Jan., pp. 501-508
[10] Budihardjo, I., Morrison, G. L., Performance of Water-in-Glass Evacuated Tube Solar Water Heaters, *Solar Energy*, *83* (2009), 1, pp. 49-56
[11] Morrison, G. L., *et al*., Water-in-Glass Evacuated Tube Solar Water Heaters, *Solar Energy*, *76* (2004), 1-3, pp. 135-140
[12] Yildizhan, H., Sivrioglu, M., Exergy Analysis of a Vacuum Tube Solar Collector System Having Indirect Working Principle, *Thermal Science*, *21* (2017), 6B, pp. 2813-2825
[13] Riahi, A., Taherian, H., Experimental Investigation on the Performance of Thermosiphon Solar Water Heater in the South Caspian Sea, *Thermal Science*, *15* (2011), 2, pp. 447-456
[14] Zeghib, I., Chaker, A., Simulation of a Solar Domestic Water Heating System, *Energy Procedia*, *6 (*2011), Dec., pp. 292-301
[15] Nitsas, M. T., Koronaki, I. P., Experimental and Theoretical Performance Evaluation of Evacuated Tube Collectors under Mediterranean Climate Conditions, *Thermal Science and Engineering Progress, 8* (2018), Dec., pp. 457-469
[16] Abdelhak, O., *et al*., The CFD Analysis of Thermal Stratification in Domestic Hot Water Storage Tank during Dynamic Mode, *In Building Simulation*, *8* (2015), 4, pp. 421-429
[17] Levers, S., Lin, W., Numerical Simulation of 3-D Flow Dynamics in a Hot Water Storage Tank, *Applied Energy*, *86* (2009), 12, pp. 2604-2614
[18] Lavan, Z., Thompson, J., Experimental Study of Thermally Stratified Hot Water Storage Tanks, *Solar Energy*, *19* (1977), 5, pp. 519-524
[19] Assari, M. R., *et al*., Numerical and Experimental Study of Inlet-Outlet Locations Effect in Horizontal Storage Tank of Solar Water Heater, *Sustainable Energy Technologies and Assessments*, *25* (2018), Feb., pp. 181-190
[20] Fernandez-Seara, J., *et al*., Experimental Analysis of a Domestic Electric Hot Water Storage Tank – Part II: Dynamic Mode of Operation, *Applied Thermal Engineering*, *27* (2007), 1, pp. 137-144
[21] Shah, L. J., Furbo, S., Entrance Effects in Solar Storage Tanks, *Solar Energy*, *75* (2003), 4, pp. 337-348
[22] Raj, A. K., *et al*., The CFD Modelling of Macro-Encapsulated Latent Heat Storage System Used for Solar Heating Applications, *International Journal of Thermal Sciences*, *139* (2019), May, pp. 88-104
[23] Demain, C., *et al*., Evaluation of Different Models to Estimate the Global Solar Radiation on Inclined Surfaces, *Renewable Energy*, *50* (2013), Feb., pp. 710-721
[24] Zelzouli, K., *et al.*, Numerical and Experimental Investigation of Thermosyphon Solar Water Heater, *Energy Conversion and Management*, *78* (2014), Feb., pp. 913-922

Paper submitted: June 1, 2019
Paper revised: October 1, 2019
Paper accepted: October 5, 2019